Faraday Discussions

Green-light wavelength-selective organic solar cells for agrivoltaics: dependence of wavelength on photosynthetic rate

Journal:	*Faraday Discussions*
Manuscript ID	FD-ART-07-2023-000141.R1
Article Type:	Paper
Date Submitted by the Author:	26-Aug-2023
Complete List of Authors:	Jinnai, Seihou; Osaka University, Soft Nanomaterials Shimohara, Naoto; Osaka University, Soft Nanomaterials Ishikawa, Kazunori; Osaka University, The Institute of Scientific and Industrial Research Hama, Kento; Suwa Tokyo Science University Iimuro, Yohei ; Suwa Tokyo Science University Washio, Takashi; Osaka University Watanabe, Yasuyuki; Suwa Tokyo Science University, Ie, Yutaka; Osaka University, The Institute of Scientific and Industrial Research

ARTICLE

Green-light wavelength-selective organic solar cells for agrivoltaics: dependence of wavelength on photosynthetic rate

Received 00th January 20xx,
Accepted 00th January 20xx

DOI: 10.1039/x0xx00000x

Seihou Jinnai,*[,a,b] Naoto Shimohara,[a] Kazunori Ishikawa,[a] Kento Hama,[c] Yohei Iimuro,[c] Takashi Washio,[a] Yasuyuki Watanabe,*[,c] and Yutaka Ie*[,a,b]

There is a growing demand for the development of novel solar systems that can simultaneously solve the problems associated with both energy generation and food supply in agriculture. Green-light wavelength-selective organic solar cells (OSCs), whose transmitted blue and red light can be utilized to promote plant growth were recently reported by our group. However, the influence of wavelength variation on the photosynthetic rate in green-light wavelength-selective OSCs remains unclear. In this study, we report on the design and synthesis of new electron-accepting π-conjugated molecules containing cyclopentene-annelated thiophene with a spiro-substituted 2,7-bis(2-ethylhexyl)fluorene (FT) unit (TT-FT-ID) as a green-light wavelength-selective nonfullerene acceptor along with a reference compound TT-T-ID. Photophysical measurements indicate that the introduction of the FT unit leads to a absorption band with a small full width at half maximum in films, leading to the ability to fine-tune the absorption length. Concerning the optimization of the conditions for the fabrication of the active layers, which are composed of a green-light wavelength-selective donor polymer of poly(3-hexylthiophene) (P3HT) and new acceptors, Bayesian optimization based on Gaussian process regression was applied to minimize the experimental batches. The green-light wavelength selective factor (S_G) and the PCEs in the green-light region (PCE-GR) of the P3HT:TT-FT-ID-based device were determined to be 0.52 and 8.6%, respectively, which are higher values than those of the P3HT:TT-FT-ID blend film. The P3HT:TT-FT-ID blend film increased the photosynthetic rate of green pepper compared to that of the P3HT:TT-FT-ID blend film. These results indicate that the fine-tuning of the absorbance required for crop growth is an important issue in developing green-light wavelength-selective OSCs for agrivoltaics.

Introduction

Solar photovoltaic systems are gaining considerable attention as a renewable energy source for the realization of sustainable societies, and silicon solar cells have been widely installed on mega solar power generation systems and the rooftops of houses.[1,2] Organic solar cells (OSCs) offer distinct advantages over silicon solar cells, including light weight, flexibility, designability, and disposability.[3-9] The typical active layer of an OSC consists of a nanometer-scale bulk hetero-junction (BHJ) structure comprised of donors (p-type organic semiconductors) and acceptors (n-type organic semiconductors).[10-13] The advantage of organic semiconductors is that the energy levels of the highest occupied molecular orbital (HOMO) and the lowest unoccupied molecular orbital (LUMO), and energy gap (E_g) can be fine-tuned through appropriate molecular design. Thus, the combination of large E_g donor polymers with small E_g nonfullerene acceptors (NFAs) becomes rational strategy for covering the entire visible light region (Fig. 1a), reaching power conversion efficiencies (PCEs) of 19%.[14-18] In contrast, it is possible to produce green-light wavelength-selective OSCs by aligning to the same E_gs between the donor and acceptor, thus producing a narrow-range wavelength absorption in the visible light region and concomitant transmission at the remaining blue and red wavelength regions (Fig. 1b). Considering the fact that representative photosynthetic dyes of chlorophyll *a* and chlorophyll *b* absorb blue and red light[19,20] (Fig. 1c), we recently reported that green-light wavelength-selective OSCs are ideal candidates for use in agrivoltaics in the greenhouse.[21] Green-light wavelength-selective OSCs can generate electricity by using the energy in the green light region, while the transmitted blue and red light can be utilized to grow crops. To realize this concept, we selected a practical and cost-effective poly-3-hexylthiophene (P3HT) as the donor,[22-30] because P3HT has a selective absorption in the green wavelength region (Fig. 1c).[31] We designed and developed a new green-light wavelength selective NFA (SNTz-RD, Fig. 2a) and reported that P3HT:SNTz-RD blend

[a] The Institute of Scientific and Industrial Research (SANKEN), Osaka University, 8-1 Mihogaoka, Ibaraki, Osaka 567-0047, Japan
[b] Innovative Catalysis Science Division, Institute for Open and Transdisciplinary Research Initiatives (OTRI), Osaka University, 2-1 Yamadaoka, Suita, Osaka 565-0871, Japan
[c] Department of Mechanical and Electrical Engineering, Faculty of Engineering, Suwa University of Science, 5000-1 Toyohira, Chino, Nagano 391-0292, Japan
Electronic Supplementary Information (ESI) available: Detailed DFT calculations, optimization of OSC active layers, synthetic detail, NMR spectra, script for Bayesian optimization. See DOI: 10.1039/x0xx00000x

films showed an improved photosynthetic rate compared to that of a P3HT:$PC_{61}BM$ film.[21] However, the influence of wavelength selectivity on the photosynthetic rate remains unclear.

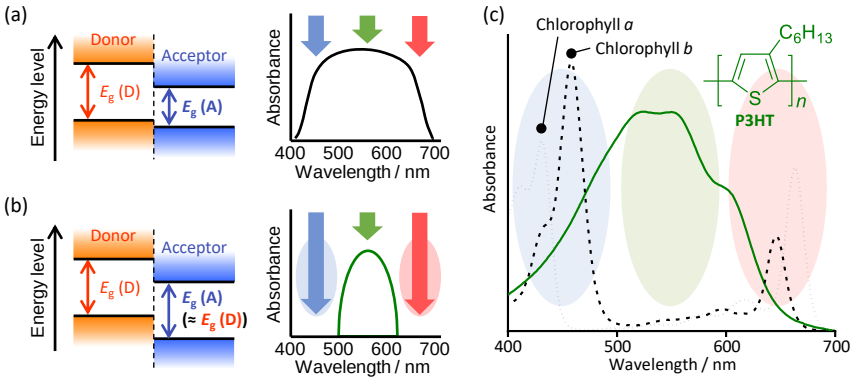

Fig. 1 Energy diagrams and corresponding absorption spectra for (a) conventional OSCs and (b) green-light wavelength-selective OSCs, and (c) absorption spectra of P3HT[31] and the chlorophylls.[20]

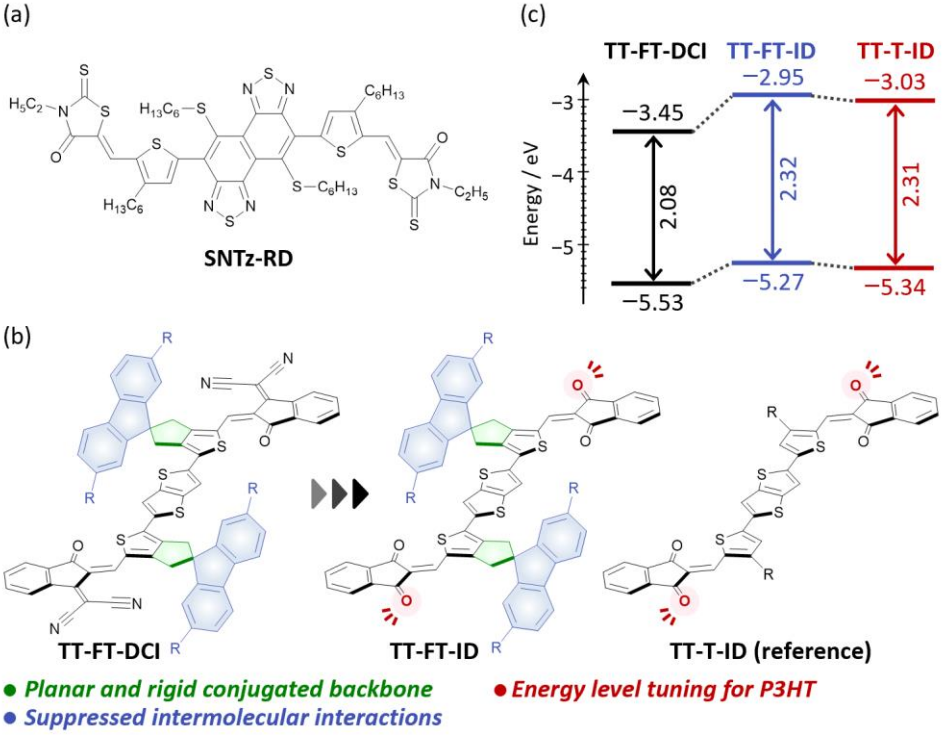

Fig. 2 Chemical structures of (a) SNTz-RD, (b) TT-FT-DCI, TT-FT-ID, and TT-T-ID. (c) Calculated energy levels of HOMOs, LUMOs, and energy gaps.

We recently reported on the development of a non-fused NFA TT-FT-DCI, which contains a cyclopentene-annelated thiophene unit with a spiro-substituted 2,7-bis(2-ethylhexyl)fluorene (FT) as a central unit and an electron-withdrawing dicyanomethylidene indanone (DCI) unit as a terminal unit (Fig. 2b).[29] The introduction of the FT unit was found to be effective in making the π-conjugated skeleton more rigid and suppressing the formation of undesired H-aggregates. The resulting absorption spectrum of the TT-FT-DCI when incorporated into films showed a wavelength-selective response with a small full width at half maximum (FWHM). We also found that the introduction of the FT unit is effective for photocarrier generation and charge transport in the BHJ active layer when combined with a representative donor-acceptor type donor polymer (PDBD-T). These features make it potentially good candidate for an acceptor of green-light wavelength-selective OSCs. Thus, by combining the relatively high-lying HOMO and LUMO energy levels of P3HT, a new NFA of TT-FT-ID and its reference compound TT-T-ID were designed by incorporating a relatively less electron-withdrawing 1,3-indanone (ID) as a terminal unit (Fig. 2b).[32,34] As shown in Fig. 2c, density functional theory (DFT) calculations using model compounds indicate that both TT-FT-ID and TT-T-ID possess higher LUMO and HOMO energy levels than those of TT-FT-DCI. In addition, the E_gs of TT-FT-ID (2.32 eV) and TT-T-ID (2.31 eV) are wider than that of TT-FT-DCI (2.08 eV) (The details of calculated results such as optimized geometries, molecular orbitals, and their energy levels for

model compounds, are provided in the Electronic Supplementary Information (ESI)). We concluded that these frontier molecular orbital energy levels of TT-FT-ID and TT-T-ID make them suitable for being combined with P3HT.[35,36] To investigate the influence of absorption range on photosynthetic rate, we also utilized TT-T-ID as a reference compound, because TT-T-ID would be expected to show red-shifted absorption in the solid state due to intermolecular interactions. In this contribution, the synthesis, physical properties, OSC characteristics, and photosynthetic rates of these compounds were investigated and the influence of wavelength range on the potential for green-light wavelength-selective OSCs was investigated.

To install such green-light wavelength-selective OSCs into greenhouses, it will be necessary to fabricate meter-scale OSC modules. Given this need, optimization of the OSC fabrication conditions becomes a major issue in terms of material usage and research resources. Therefore, in this research, Bayesian optimization (BO) based on Gaussian process regression (GPR) was preliminarily used to examine the optimization of the OSC active layers.[37-39]

Results and discussion

Synthesis.

The target compounds TT-FT-ID and TT-T-ID were synthesized by Knoevenagel condensation reactions from known compounds 1 and 2, respectively (Scheme 1).[32] TT-FT-IID and TT-T-ID were sufficiently soluble in representative film-processing solvents such as chloroform ($CHCl_3$), chlorobenzene, and *o*-dichlorobenzene. Detailed information on the synthesis and characterization of the materials are summarized in the ESI.

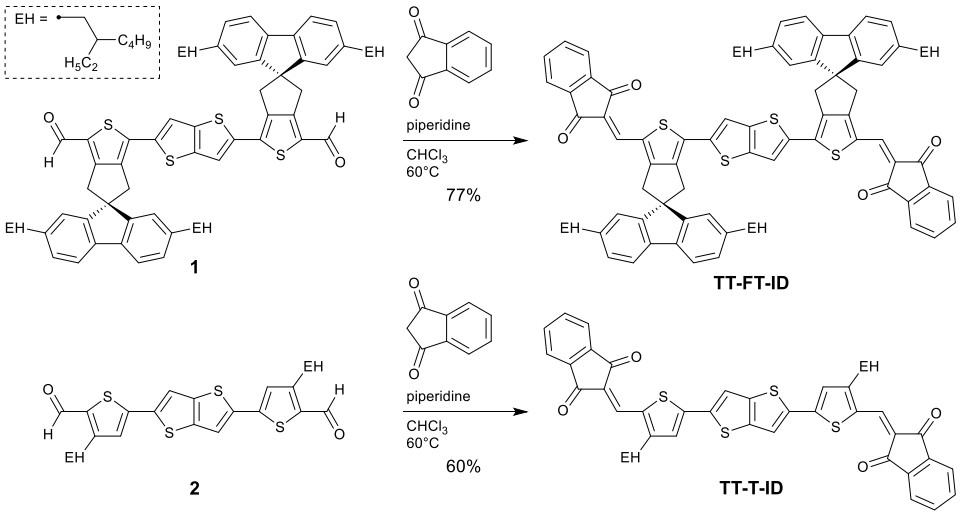

Scheme 1 Synthetic routes for the target compounds.

Photophysical properties.

The absorption spectra of TT-FT-ID and TT-T-ID in $CHCl_3$ solutions showed that both compounds exhibit absorption bands in the green wavelength range of 500-600 nm, and absorption intensities in the blue (400-500 nm) and red (600-700 nm) wavelength regions are relatively low (Fig. 3a and b). Photophysical data are collected in Table 1. These absorption spectra are favorable for making the compounds useful for use in green-light selective organic semiconducting materials. The maximum absorption wavelengths (λ_{max}s) of TT-FT-ID and TT-T-ID were observed at 604 and 541 nm, respectively. The λ_{max} of TT-FT-ID is red-shifted compared to that of TT-T-ID, which can be attributed to the rigidified π-conjugated backbone of TT-FT-ID.[32] The TT-FT-ID and TT-T-ID thin films were fabricated by spin-coating on a quartz plate, and their absorption spectra in films were measured. As shown in Fig. 3, the absorption band of TT-FT-ID in a film was almost superimposable with that in solution, whereas an apparent red-shift was observed for TT-T-ID. Furthermore, the full width at half maximum (FWHM) of the absorption band of the TT-FT-ID in films (146 nm) was smaller than that of TT-T-ID (181 nm). These phenomena reflect the different degree of intermolecular interactions in films: the presence of the FT backbone suppresses the formation of H-aggregates for TT-FT-ID, whereas molecular stacking arrangements are formed for TT-T-ID. The optical energy gaps (ΔE_{opt} (film)) estimated from the onset of the absorption spectrum were determined to be 1.82 eV for TT-FT-ID and 1.78 eV for TT-T-ID, respectively.

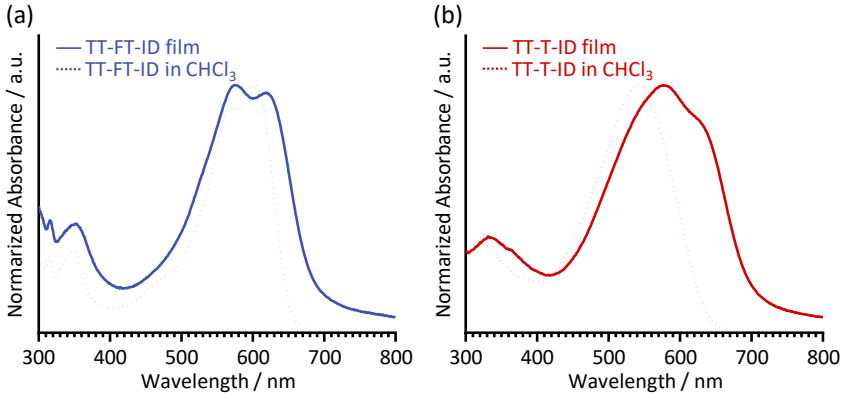

Fig. 3 UV-vis absorption spectra in films (solid lines) and in $CHCl_3$ solutions (dotted lines) for (a) TT-FT-ID and (b) TT-T-ID.

Table 1. Physical properties of TT-FT-ID and TT-T-ID.

compound	λ_{max} (sol.) / nm[a]	λ_{max} (film) / nm	ΔE_{opt} (film) / nm[b]	FWHM[c] / nm	EA / eV[d]	IP / eV[e]
TT-FT-ID	604	575	1.82	146	3.62	5.58
TT-T-ID	541	577	1.78	181	3.36	5.31

[a] In $CHCl_3$. [b] Determined from the onset values of the UV–vis absorption spectra. [c] Calculated for the absorption spectra of thin-films. [d] Determined by LEIPS. [e] Determined by PYS.

Physicochemical properties.

The electron affinities (EAs) and ionization potentials (IPs) of TT-FT-ID and TT-T-ID in films were determined using low-energy inverse photoemission spectroscopy (LEIPS)[40] and photoelectron yield spectroscopy (PYS)[41,42] (Fig. 4). The EA values for TT-FT-ID and TT-T-ID were estimated to be 3.62 and 3.36 eV from the onset energy levels for the LEIPS spectra. The IP values were found to be 5.58 eV for TT-FT-ID and 5.31 eV for TT-T-ID, respectively (Table 1). These estimated energy levels indicate that TT-FT-ID and TT-T-ID can function as acceptors when combined with P3HT in OSCs.[35,36]

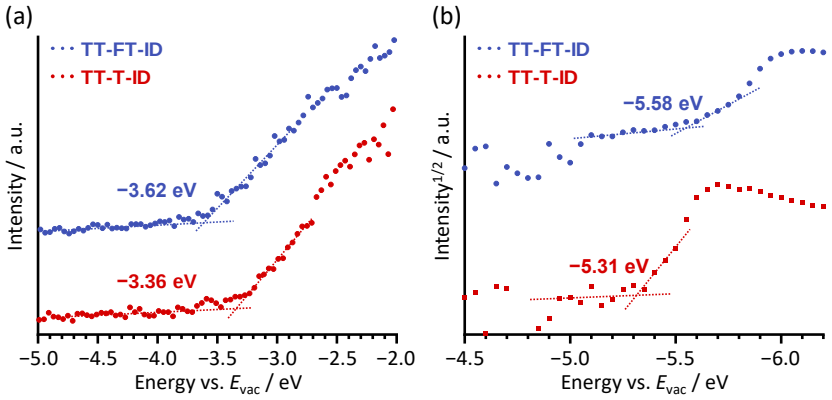

Fig. 4 (a) LEIPS and (b) PYS spectra for TT-FT-ID (blue) and TT-T-ID (red) thin-films.

OSC characteristics.

The OSC characteristics of TT-FT-ID and TT-T-ID were evaluated using an inverted device configuration of indium tin oxide (ITO)/ZnO/P3HT:acceptor/MoO_3/Ag.[43] It is known that the intermixing between donor and acceptor, that the crystallinity, and morphologies of the active layers largely depend on the fabrication conditions. Thus, to obtain the best OSC characteristics, many factors such as donor:acceptor ratio, process solvent, thermal annealing, concentration, and the rotational speed of spin-coating need to be precisely optimized. In this study, we effectively utilized GPR to decrease the number of experimental optimizations. The GPR model is a nonparametric kernel-based stochastic model, which is a major machine learning algorithm that is useful for searching for optimal conditions for black-box functions such as active layer fabrication conditions for OSCs.[37-39] We initially determined the P3HT:acceptor ratio and process solvent to be 1.5:1 and DCB, respectively (Table S1 and S2). The solvent concentration and rotational speed, whose precise balance is generally crucial for producing desired films was then optimized by

GPR to minimize the experimental costs. To calculate the mean function and variance function of GPR, we initially tested 10 conditions to obtain datasets for P3HT:TT-FT-ID and P3HT:TT-T-ID, respectively (Table S3 and S4). The mean functions and variance functions for thePCE of P3HT:TT-FT-ID and P3HT:TT-T-ID devices were calculated by GPR using the Matérn kernel 5/2 (Fig. 5).[37] The r range for rotational speed was examined between 500 and 5000 rpm. Concentration was examined in the range of 5 ~ 40 mg/mL for P3HT:TT-FT-ID and 5 ~ 20 mg/mL for P3HT:TT-T-ID, respectively. As shown in Fig. 5a and 5d, the mean functions showed clear trends for the concentration and rotational speed, indicating that the optimum conditions were included within the dotted line area. The fabrication conditions for the active layer for the next batches were suggested and examined based on an upper confidence bound (UCB) mode of GPR derived from the mean functions and variance functions (Fig. 5c and Fig. 5f). As shown in Table S5, the first-order prediction of 1.96% from the small data set in Table S3 was sufficiently close to the experimental value of 2.04%. We therefore concluded that optimization of the fabrication conditions for the P3HT:TT-FT-ID-based OSC device was efficiently conducted by the GPR method by one batch of dataset construction and one batch of optimization experiments (Table S5 and S6). On the other hand, although high PCEs were predicted at high concentrations of the P3HT:TT-T-ID-based OSC device (Fig. 5d), the reproducibility of the formation for the P3HT:TT-T-ID films under high concentration conditions over 20 mg mL^{-1} was low due to the relatively low solubility of TT-T-ID.

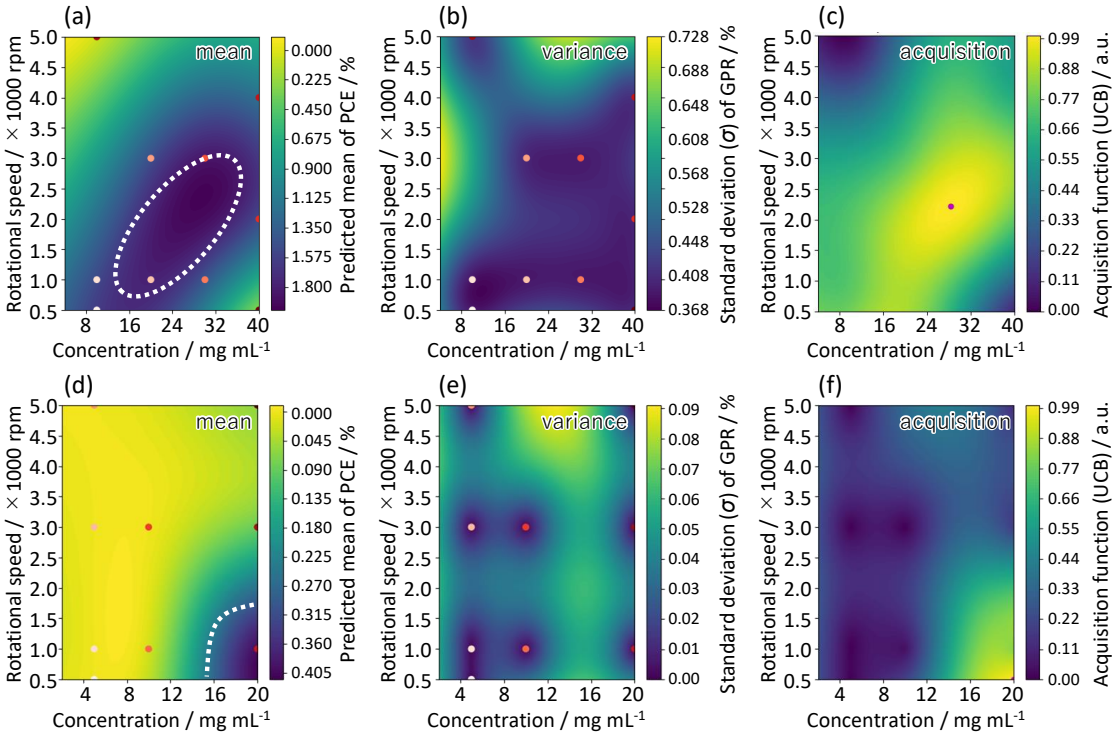

Fig. 5 GPR for the P3HT:TT-FT-ID and P3HT:TT-T-ID devices. The estimated mean PCE (a and d) and variance (b and e) were calculated based on the Matérn kernel 5/2. The high performance region predicted by GPR are indicated by dotted areas. The acquisition functions (c and f) were calculated by the UCB mode of GPR. Appropriate conditions were indicated by red point. The Python source code for GPR is supplied in the ESI.

The current density (*J*)–voltage (*V*) characteristics of the optimized OSCs under AM 1.5 G solar irradiation (100 mW cm^{-2}) and the corresponding external quantum efficiency (EQE) spectra are shown in Fig. 6a and b. The representative OSC parameters for the short-circuit current (J_{SC}), open-circuit voltage (V_{OC}), and fill factor (FF) are summarized in Table 2. The best OSC characteristics of the P3HT:TT-FT-ID and P3HT:TT-T-ID blend films were found to be 2.43% and 0.55%, and the average PCE values were determined to be 2.15 ± 0.26% and 0.40 ± 0.11%, respectively. The PCE values for the P3HT:TT-FT-ID-based OSC device were approximately 4 times higher than that of the P3HT:TT-T-ID-based OSCs. Among the OSC parameters, the J_{SC} values showed a substantial improvement. This trend is consistent with our recent report on an acceptor that contained FT units.[32] The surface morphologies of the active layers were investigated by atomic force microscopy (AFM). As shown in Fig. 8, the P3HT:TT-FT-ID blend films had a smooth surface morphology with a mean square roughness (R_{rms}) of 1.68 nm (Fig. 7a), whereas the P3HT:TT-T-ID blend films had a more distinct grain structure with an R_{rms} of 11.6 nm (Fig. 7b). We assume that this difference in surface morphologies reflects the aggregation behavior of the acceptors: the tendency of TT-T-ID to form intermolecular aggregates results in excessive grain formation in the blend films, while the introduction of the FT unit into TT-FT-ID contributes to the suppression of excessive grain formation. We conclude that the nanometer-scale smooth morphologies are advantageous for the efficient generation of photocarriers, resulting in higher J_{SC} values for the P3HT:TT-FT-ID blend films.

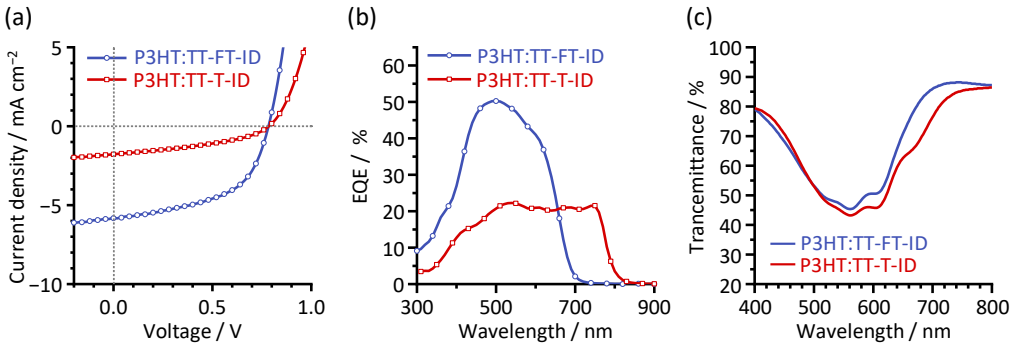

Fig. 6 (a) *J–V* curves and (b) EQE spectra of the OSC devices. (c) Transmittance spectra of blend films.

Table 2. OSC characteristics of P3HT:TT-FT-ID and P3HT:TT-T-ID based devices.

acceptor	J_{SC} / mA cm^{-2}	V_{OC} / V	FF / %	PCE / %	EQE_{max} / %	S_G[a]	PCE-GR[a] / %
TT-FT-ID	5.83 (5.70 ± 0.74)	0.78 (0.78 ± 0.01)	53 (49 ± 5)	2.43 (2.15 ± 0.26)	50	0.52	8.6
TT-T-ID	1.78 (1.38 ± 0.27)	0.79 (0.74 ± 0.07)	39 (38 ± 2)	0.55 (0.40 ± 0.11)	22	0.45	3.2

[a] Calculated according to the equation in Ref. 21.

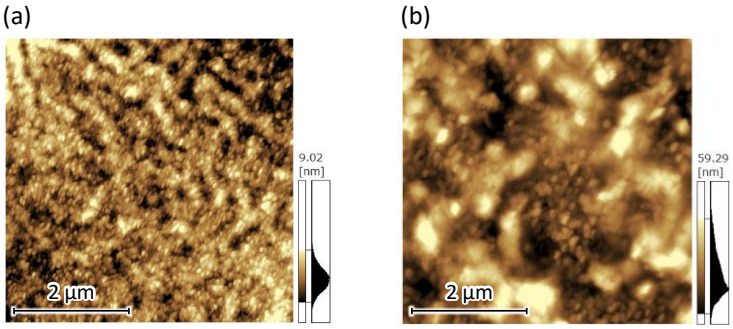

Fig. 7 AFM images of (a) P3HT:TT-FT-ID and (b) P3HT:TT-T-ID films.

Green-light wavelength-selective properties and photosynthetic rate measurements.

We recently proposed that the green-light wavelength selective factor (S_G) be used as an index of the blend films for green-light wavelength selective OSCs.[21] This S_G becomes 0 when the transmittance spectrum in the range from 400 to 700 nm is completely flat (no selectivity). On the other hand, the S_G approaches 1 when the contribution to the transmittance in the blue and red wavelength regions increases. Based on the transmittance spectra of the P3HT:TT-FT-ID and P3HT:TT-T-ID blend films (Fig. 6c), the S_G values were determined to be 0.52 and 0.45, respectively. The P3HT:TT-FT-ID film showed a larger S_G value compared to that of the P3HT:TT-T-ID film, indicating an increase in green-light wavelength selectivity for the P3HT:TT-FT-ID film. The origin of the larger S_G of the P3HT:TT-T-ID film can be attributed to the suppressed red-shift in the absorption and the narrow FWHM of TT-FT-ID in films (Table 1). It should also be noted that the S_G of the P3HT:TT-FT-ID film was larger than that of our previously reported P3HT:SNTz-RD film (S_G = 0.44).[21] This improvement is mainly due to the increased transmittance in the blue-light wavelength region. To quantitatively evaluate the photovoltaic characteristics of these materials for agrivoltaics, we also proposed the use of PCEs in the green-light region (PCE-GR) as a benchmark for energy utilization efficiency in the green wavelength region. As a result of the larger S_G and higher PCE values, the P3HT:TT-FT-ID-based OSCs showed a superior PCE-GR value of 8.6%, compared to those of the P3HT:TT-T-ID-based OSCs (PCE-GR = 3.2%) and the P3HT:SNTz-RD-based OSCs (PCE-GR = 5.8%).

To investigate the influence of wavelength range on the potential of these green-light wavelength-selective OSCs, the photosynthetic rates for green pepper under artificial sunlight through the blend films were evaluated using gas exchange experiments.[21] The light saturation point of green pepper is reported to be 20–30 klx, corresponding to around 600-800 μmol·m^{-2}·s^{-1}.[44] This value is approximately half of that which is typically required for tomatoes and melons, which are commonly grown in greenhouses. Therefore, we concluded that the green pepper would be a suitable crop for green-light wavelength selective OSCs. Fig. 8 shows the average photosynthetic rates for 4 measurements under each condition. We utilized the same

green pepper for these measurements to suppress the deviations that depend on the differences in pepper seedlings. The results for the individual measurements and plots with standard deviation are provided in Tables S9–S11 and Fig. S2 in the ESI. The photosynthetic rates under the P3HT:TT-FT-ID and P3HT:TT-T-ID blend films were smaller than that under that for the control conditions (*i.e.*, a glass substrate without an active layer). However, it should be emphasized that the photosynthetic rate of the P3HT:TT-FT-ID blend film was larger than that of the P3HT:TT-T-ID blend film. When we look closer at Fig. 6c, the transmission spectrum of P3HT:TT-T-ID showed a shoulder at around 650-700 nm, which we attribute to the aggregation of the TT-T-ID. In contrast, this shoulder was not observed for the P3HT:TT-FT-ID blend films, thus resulting in improved transmittance in the 650-700 nm region. This wavelength region overlaps with the Q-band of porphyrin-based chlorophylls *a* and *b*. We therefore conclude that the P3HT:TT-FT-ID blend film resulted in an improved photosynthetic rate because of the increased transmittance in the Q-band region. This result suggests that a narrow absorption wavelength of less than 650 nm might be an effective strategy for balancing between power generation and crop cultivation.

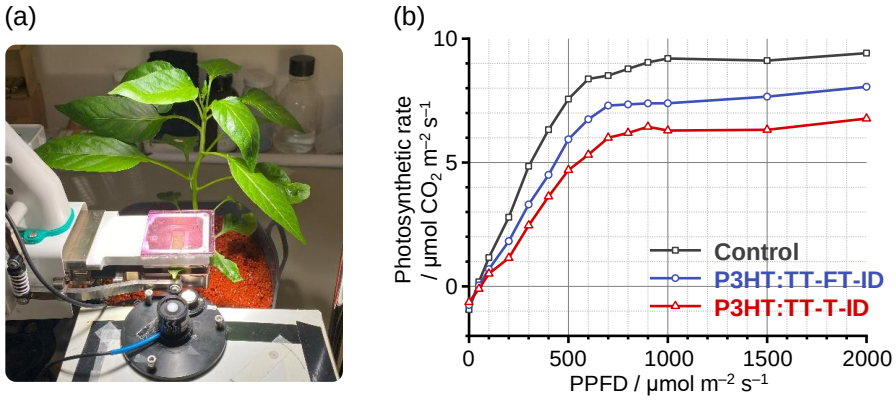

Fig. 8 (a) Photo of the photosynthesis experiments. (b) Photosynthetic rates of green pepper under each light condition.

Conclusions

In summary, to develop green-light wavelength-selective OSCs for use in agrivoltaics, new nonfullerene acceptors TT-FT-ID along with TT-T-ID were successfully designed and synthesized. Photophysical measurements indicate that both the TT-FT-ID and TT-T-ID in films resulted in one absorption band in the green-wavelength region, and TT-FT-ID showed an absorption band with a smaller FWHM due to the introduction of the FT unit. The electron affinities of these compounds were found to be suitable for use in combination with P3HT due to the introduction of the relatively weak electron-withdrawing group of ID as the terminal unit. For the fabrication of the active layers of OSCs, solution concentration and rotation speed could be sufficiently optimized in one dataset construction experiment and one optimization experiment. The P3HT:TT-FT-ID films showed OSC characteristics with 8.6% PCE-GR, whose value is better than those of TT-T-ID and of our previously reported SNTz-RD. The S_G values of the P3HT:TT-FT-ID films were slightly larger that of P3HT:TT-T-ID, reflecting an absorption spectrum with a small FWHM. Measurement of the photosynthetic rate using green pepper indicated that the the photosynthetic rates for the P3HT:TT-FT-ID film were increased compared to that of the P3HT:TT-T-ID film. These results demonstrate that the electron-accepting π-conjugated molecules with selective green-light absorption and high OSC characteristics represent potential candidates for green-light wavelength-selective nonfullerene acceptors for agrivoltaics. To further clarify the relationship between green-light wavelength selectivity and crop growth, investigations on crop growing by the green-light wavelength selective OSCs is currently underway in our group.

Experimental

OSC device fabrication and evaluation.

OSC devices with a structure of ITO/ZnO/P3HT:acceptor/MoO_3/Ag were prepared.[43] ITO-coated glass substrates were sonicated in acetone, water, and 2-propanol for 10 min, respectively. The resulting ITO-coated glass substrates were then treated with O_3 for 30 min in a UV/O_3 cleaner (Filgen Inc., UV253). A ZnO layer was spin-coated using a solution of zinc acetate dihydrate (99.9%, 200 mg), ethanolamine (99%, 55 μL), and 2-methoxyethanol (99.8%, 2 mL) at 4000 rpm using a spin coater (MIKASA Co., Ltd., MS-A100) and then baked at 200 °C for 30 min in an ambient atmosphere. The active layer was then formed by spin-coating on the ITO/ZnO electrode. The fabrication conditions, such as P3HT:acceptor weight ratio, solvent, concentration, rotational speed, and w/o thermal annealing are listed in Table S1–6 in the ESI. MoO_3 and Ag electrodes were evaporated on the top of active layer through a shadow mask to define the active area of the devices (0.09 cm^2) under a high vacuum of 10^{-5} Pa to a thickness of 10, 80 nm, as determined by a quartz crystal monitor. After sealing the device from the air, the photovoltaic characteristics were

measured in air under simulated AM 1.5G solar irradiation (100 mW cm^{-2}) (SAN-EI ELECTRIC, XES-301S). The current density–voltage characteristics of the photovoltaic devices were measured by means of a KEITHLEY 2400 source meter. The EQE spectra were measured by using a Soma Optics Ltd. S-9240.

Photosynthesis evaluation.

Photosynthetic rates were determined by gas exchange experiments using an Li-6800 photosynthesis system (LICAR) and a SOLAX series XC-100EF light source (SERIC Ltd., Japan). The OSC films of P3HT:TT-FT-ID and P3HT:TT-T-ID were prepared on a glass substrate by spin-coating and subsequent sealing from the air with a cover glass. The light saturation point (LSP) and photosynthetic rate were evaluated at a controlled temperature of 25 °C and a CO_2 concentration of 400 ppm.

Conflicts of interest

There are no conflicts to declare.

Acknowledgements

This work was supported by JSPS KAKENHI (20H02814, 20H05841, 20KK0123, 20K15352, and 23H02064), JST (22713577) and from The Ministry of Education, Culture, Sports, Science and Technology, Japan. This work was also supported by JST, CREST (Grant Number JPMJCR1666, 20343768), Japan. We acknowledge to the support of AIRC center, SANKEN, Osaka University. We also acknowledge to Nanotechnology Open Facilities, Osaka University (JPMXP09S21OS0010) for photoelectron yield spectroscopy measurements. We are thankful to Mr. Hiroki Mori for the assistance of LEIPS measurements and Mr. Masahiro Suzuki and Syou Mochiduki for the assistance of photosynthetic rate measurements. We are also thankful to the CAC, SANKEN, for the elemental analyses and for collecting the high-resolution mass spectra.

Notes and references

1 K. Bóddis, I. Kougias,A. Jäger-Waldau, N. Taylor and S. Szabó, *Renew. Sustain. Energy Rev.*, 2019, **114**, 109309.
2 P. Gagnon, R. Margolis, J. Melius, C. Philips and R. Elmore, *Rooftop Solar Photovoltaic Technical Potential in the United States: A Detailed Assessment., NREL Technical Report*, NREL/TP-6A20-65298, Unitad States, 2016.
3 A. Polman, M. Knight, E. C. Garnett, B. Ehrler and W. C. Sinke, *Science*, 2016, **352**, aad4424.
4 O. Inganäs, *Adv. Mater.*, 2018, **30**, 1800388.
5 C. Liu, C. Xiao, C. Xie and W. Li, *Nano Energy*, 2021, **89**, 106399.
6 P. Cheng and X. Zhan, *Chem. Soc. Rev.*, 2016, **45**, 2544–2582.
7 R. R. Søndergaad, N. Espinosa, M. Jørgensen and F. C. Krebs, *Energy Environ. Sci.*, 2014, **7**, 1006–1012.
8 Y. Zhou, C. Fuentes-Hernandez, T. M. Khan, J.-C. Liu, J. Hsu, J. W. Shim, A. Dindar, J. P. Youngblood, R. J. Moon and B. Kippelen, *Sci. Rep.*, 2013, **3**, 1536.
9 T. Takada, T. Uchiyama, Y. Okada-Shudo, K. Hoshino, K. Koizumi, Y. Takeoka and V. Vohra, *ACS Sustain. Chem. Eng.*, 2020, **8**, 5807–5814.
10 G. Yu, J. Gao, J. C. Hummelen, F. Wudl and A. J. Heeger, *Science*, 1995, **270**, 1789–1791.
11 J. J. M. Halls, K. Pichler, R. H. Friend, S. C. Moratti and A. B. Holmes, *Appl. Phys. Lett.*, 1996, **68**, 3120–3122.
12 G. Zhang, J. Zhao, P. C. Y. Chow, K. Jiang, J. Zhang, Z. Zhu, J. Zhang, F. Huang and H. Yan, *Chem. Rev.*, 2018, **118**, 3447–3507.
13 H. Imahori, Y. Kobori and H. Kaji, *Acc. Chem. Res.*, 2021, **2**, 501–514.
14 Y. Lin, J. Wang, Z. G. Zhang, H. Bai, Y. Li, D. Zhu and X. Zhan, *Adv. Mater.*, 2015, **27**, 1170–1174.
15 W. Zhao, D. Qian, S. Zhang, S. Li, O. Inganäs, F. Gao and J. Hou, *Adv. Mater.*, 2016, **28**, 4734–4739.
16 J. Yuan, Y. Zhang, L. Zhou, G. Zhang, H.-L. Yip, T.-K. Lau, X. Lu, C. Zhu, H. Peng, P. A. Johnson, M. Leclerc, Y. Cao, J. Ulanski, Y. Li and Y. Zou, *Joule*, 2019, **3**, 1140–1151.
17 L. Zhan, S. Li, Y. Li, R. Sun, J. Min, Z. Bi, W. Ma, Z. Che, G. Zhou, H. Zh, M. Shi, L. Zuo and H. Chen, *Joule*, 2022, **6**, 662–675.
18 Y. Cui, Y. Xu, H. Yao, P. Bi, L. Hong, J. Zhang, Y. Zu, T. Zhang, J. Qin, J. Ren, Z. Chen, C. He, X. Hao, Z. Wei and J. Hou, *Adv. Mater.*, 2021, **33**, 2102420.
19 L. O. Björn, G. C. Papageorgios, R. E. Blankenship and Govindjee, *Photosynth. Res.*, 2009, **99**, 85–98.
20 L. A. Clementson and B. Wojtasiewicz, *Data Br.*, 2019, 24, 103875.
21 S. Jinnai, A. Oi, T. Seo, T. Moriyama, M. Terashima, M. Suzuki, K.-i. Nakayama, Y. Watanabe and Y. Ie, *ACS Sustain. Chem. Eng.*, 2023, **11**, 1548–1556.
22 M. T. Dang, L. Hirsch and G. Wantz, *Adv. Mater.*, 2011, **23**, 3597–3602.
23 Q. Wang, Y. Qin, M. Li, L. Ye and Y. Geng, *Adv. Energy Mater.*, 2020, **10**, 2002572.
24 T. M. Pappenfus, F. Almyahi, N. A. Cooling, E. W. Culver, S. C. Rasmussen and P. C. Dastoor, *Macromolecular Chem. Phys.*, 2018, **219**, 1800272.
25 R. Po, A. Bernardi, A. Calabrese, C. Carbonera, G. Corso and A. Pellegrino, *Energy Environ. Sci.*, 2014, **7**, 925–943.
26 S. Chatterjee, S. Jinnai and Y. Ie, *J. Mater. Chem. A*, 2021, **9**, 18857–18886.
27 S. Chatterjee, T. Ohto, H. Tada, S. Jinnai and Y. Ie, *ACS Sustain. Chem. Eng.*, 2020, **8**, 19013–19022.
28 S. Chatterjee, Y. Ie, M. Karakawa and Y. Aso, *Adv. Funct. Mater.*, 2016, **26**, 1161–1168.
29 S. Chatterjee, Y. Ie, T. Seo, T. Moriyama, G.-J. A. H. Wetzelaer, P. W. M. Blom and Y. Aso, *NPG Asia Mater.*, 2018, **10**, 1016–1028.

30 S. Jinnai and Y. Ie, *J. Photopolym. Sci. Tech.*, 2021, **34**, 285–290.
31 S. Jinnai, Y. Ie, M. Karakawa, T. Aernouts, Y. Nakajima, S. Mori and Y. Aso, *Chem. Mater.*, 2016, **28**, 1705–1713.
32 S. Jinnai, K. Murayama, K. Nagai, M. Mineshita, K. Kato, A. Muraoka, A. Yamakata, A. Saeki, Y. Kobori and Y. Ie, *J. Mater. Chem. A*, 2022, **10**, 20035–20047.
33 K. N. Winzenberg, P. Kemppinen, F. H. Scholes, G. E. Collis, Y. Shu, T. B. Singh, A. Bilic, C. M. Forsyth and S. E. Watkins, *Chem. Commun.*, 2013, **49**, 6307–6309.
34 Suman and S. P. Singh, *J. Mater. Chem. A*, 2019, **7**, 22701–22729.
35 C. B. Nielsen, S. Holiday, H.-Y. Chen, S. J. Cryer and I. McCulloch, *Acc. Chem. Res.*, 2015, **48**, 2803–2812.
36 Q. Yue, W. Liu and X. Zhu, *J. Am. Chem. Soc.*, 2020, **142**, 11613–11628.
37 T. Osterrieder, F. Schmitt, L. Luer, J. Wagner, T. Heumüller, J. Hauch and C Brabec, *arXiv*, 2023, DOI: 10.48550/arXiv.2305.08248.
38 M. Kondo, H. D. P. Wathsala, M. Sako, Y. Hanatani, K. Ishikawa, S. Hara, T. Takaai, T. Washio, S. Takizawa and H. Sasai, *Chem. Commun.*, 2020, **56**, 1259–1262.
39 Y. Naito, M. Kondo, Y. Nakamura, N. Shida, K. Ishikawa, T. Washio, S. Takizawa and M. Atobe, *Chem. Commun.*, 2022, **58**, 3893–3896.
40 H. Yoshida, *Chem. Phys. Lett.*, 2012, **539–540**, 180–185.
41 R. Grzibovskis and A. Vembris, *J. Mater. Sci.*, 2018, **53**, 7506–7515.
42 H. Ishii, H. Kinjo, T. Sato, S.-i. Machida and Y. Nakayama, *Photoelectron Yield Spectroscopy for Organic Materials and Interfaces*, Springer, Tokyo, Japan, 2015, Ch. 8, pp. 131–155.
43 A W. Zhao, S. Li, H. Yao, S. Zhang, Y. Zhang, B. Yang and J. Hou, *J. Am. Chem. Soc.*, 2017, **139**, 7148–7151.
44 T. Sekiyama and A. Nagashima, *Environ.*, 2019, **6**, 65.